

# Bayesian Optimization Parameter Tuning Framework for a Lyapunov Based Path Following Controller

Zhewen Zheng<sup>a</sup>, Wenjing Cao<sup>a</sup>, Hongkang Yu<sup>a</sup>, Mo Chen<sup>b</sup>, Takashi Suzuki<sup>a</sup>,

arXiv:2512.12649v1 [cs.RO] 14 Dec 2025

**Abstract**—Parameter tuning in real-world experiments is constrained by the limited evaluation budget available on hardware. The path-following controller studied in this paper reflects a typical situation in nonlinear geometric controller, where multiple gains influence the dynamics through coupled nonlinear terms. Such interdependence makes manual tuning inefficient and unlikely to yield satisfactory performance within a practical number of trials. To address this challenge, we propose a Bayesian optimization (BO) framework that treats the closed-loop system as a black box and selects controller gains using a Gaussian-process surrogate. BO offers model-free exploration, quantified uncertainty, and data-efficient search, making it well suited for tuning tasks where each evaluation is costly. The framework is implemented on Honda’s AI-Formula three-wheeled robot and assessed through repeated full-lap experiments on a fixed test track. The results show that BO improves controller performance within 32 trials, including 15 warm-start initial evaluations, indicating that it can efficiently locate high-performing regions of the parameter space under real-world conditions. These findings demonstrate that BO provides a practical, reliable, and data-efficient tuning approach for nonlinear path-following controllers on real robotic platforms.

**Index Terms**—Class, IEEEtran, LATEX, paper, style, template, typesetting.

## I. INTRODUCTION

PATH following control is the cornerstone of autonomous navigation for mobile robots. The path following controller provides sufficient steering input as well as throttle and braking input to control the direction and speed of the robot to guide the controlled robot along a pre-defined path [1], [2]. Across all categories of controllers, one practical challenge in real-world applications is parameter tuning, since improper parameter settings can lead to a significant decline in system performance [3], [4]. PID (and sometimes PI) is the most widely used path following control method in industrial applications. PID gains are often tuned using engineering experience and iterative trial-and-error procedures, most commonly via the Ziegler–Nichols rules and the Cohen–Coon formulas [5], [6], [7]. These manual parameter tuning techniques are simple to implement and particularly effective in early-stage tuning when the number of parameters is small

Manuscript received ???; revised ???; accepted ????. Manuscript received in final form ????. This work was developed by the Control Engineering Lab, Department of Engineering and Applied Sciences, Sophia University.

Z. Zheng, W. Cao, T. Suzuki, and H. Yu are with the Department of Engineering and Applied Sciences, Sophia University, Tokyo 102-8554, Japan (e-mail: z-zheng-9n2@eagle.sophia.ac.jp; wenjing-cao@sophia.ac.jp; ????).

M. Chen is with the Department ????, Waseda University, ????, Japan (e-mail: ???).

and weakly coupled, as in PI (two gains) and PID (three gains) controllers. Despite relying on operator experience and requiring multiple iterations, manual tuning remains prevalent as a practical baseline for further refinement to achieve the desired performance.

As control and path following techniques have evolved, more advanced controllers are used to augment or replace PID to meet more demanding performance and robustness requirements. As recent representative examples, Sabiha [8] used a kinematic backstepping controller with 3 gains cascaded with an SMC layer with 5 gains. Kasim [9] designed a Lyapunov-based kinematic controller with 4 gains in polar error coordinates. Peng et al. [10] formulated an LMI-based MPC for a four-vertex LPV model with 8 scheduled state-feedback gains. Zhao et al. [11] adopted a DDPG-based controller that requires multiple reward weights, OU exploration parameters and various training hyperparameters. Compared with PID, these schemes involve a larger and more strongly coupled set of parameters, so manual tuning becomes inefficient and requires numerous closed-loop evaluations, making it difficult to locate the optimum in high-dimensional parameter spaces [12]. Consequently, a shift from ad hoc adjustment to optimal automatic controller tuning is necessary.

Given this shift, many studies turned to optimization-based techniques such as gradient-based approaches for controller tuning [13]. However, in real-world tuning, gradient-based methods often become ineffective when objectives are non-convex, noisy, or non-smooth, leading to many local extrema and unreliable gradient information. As a result, these methods become sensitive to initialization and tend to converge to a local optimum rather than a near-global optimum [14], [15]. Moreover, in multivariable nonlinear control systems, the performance index  $J$  often has no analytical form or gradient and can only be evaluated through closed-loop experiments as a black-box function. To avoid reliance on gradient information, evolutionary and other derivative-free search strategies have been explored for controller parameter tuning [16], [17], [18]. Although these approaches relax differentiability assumptions, they often require a large number of performance evaluations to identify satisfactory parameter settings. In real world experiments, each evaluation of  $J$  requires a costly closed-loop experiment, only a limited number of trials can be performed on the robot. Especially for a non-small robot platform such as the AI-Formula robot used in this study (wheelbase  $\approx 0.80$  m, track width  $\approx 0.60$  m), each closed-loop run requires substantial time and a dedicated test

environment, which further increases the experimental cost. These challenges have motivated growing interest in Bayesian Optimization (BO). [19], [20].

BO is a sequential model-based optimization method that updates a probabilistic surrogate of system performance and uses an acquisition function to select evaluation points for controller tuning. BO has three key properties: it explores the parameter space globally, achieves high sample efficiency, and remains reliable under costly or noisy physical experiments [21], [22]. Matthew Tesch *et al.* (2011) were among the first to demonstrate BO in a real-world setting by applying it to a snake robot and optimizing its gait parameters [23]. Following this early work, BO has been validated on several real-world control systems, including legged robotic platforms, industrial process actuators, and the high-pressure fuel supply system of a combustion engine [24], [25], [19].

Around 2020, BO-based parameter tuning for path following controllers first appeared in simulation studies. Gharib *et al.* used BO in simulation to tune seven cost-function weights in a MPC-based path-following controller [26], while Strózecki *et al.* applied BO in simulation to tune six weighting parameters in a MPC-based lateral controller for lane keeping [27]. These studies represent the early applications of BO to the tuning of path-following controllers for wheeled vehicles, but they remained simulation-only. BO was later extended from simulation environments to physical vehicle platforms. Fröhlich *et al.* (2022) employed contextual BO to adjust the weighting parameters of an MPCC on a 1:28 autonomous racing car, validating the tuned controller through extensive real-world laps [28]. Menn *et al.* (2024) employed a Lipschitz-safe BO scheme to tune a modified rear-axis tracking controller and confirmed its effectiveness under safety-constrained on-road testing [29]. Hence, prior work establishes the feasibility of BO-based tuning for vehicle path-following controllers. However, existing BO studies have focused almost exclusively on MPC formulations, while geometric controllers with strongly coupled parameters such as the one considered in this paper have not been examined in the BO tuning literature. Real-world BO experiments for path following controller parameter tuning also remain limited. This motivates the first contribution of this study.

This paper makes the following main contributions:

- A BO framework is proposed that treats the geometric path-following controller as a black-box closed-loop system, enabling its four strongly coupled gains to be optimized directly from real-vehicle behavior without requiring an analytical model or gradient information.
- A kinematic path-following controller derived using the Lyapunov direct method [9] is adapted from simulation to a corrected and implementation-ready closed-loop form for real-vehicle use, providing the system on which BO performs data-driven gain tuning.
- The proposed BO framework is validated through repeated track experiments on Honda's AI-Formula three-wheeled robot platform [30], demonstrating that effective gain optimization can be achieved with a limited number of real-world evaluations.

The remainder of this paper is organized as follows. Section II presents the problem formulation, including the geometric path-following controller to be tuned and the definition of the tracking-error dynamics. Section III introduces the proposed Bayesian Optimization framework for automatic controller parameter tuning. Section IV demonstrates the real-world performance of the tuned controller through experiments on the AI-Formula robot platform. Finally, Section V concludes this work and outlines potential directions for future research.

## II. PROBLEM FORMULATION

### A. AI-Formula Robot Introduction

The AI-Formula robot used in this study is a three-wheeled electric platform developed for autonomous driving research [30]. The AI-Formula project, conducted in collaboration with Honda, offers a real-world autonomous racing environment for mobility research. The robot uses front-wheel drive, and the rear wheels are passive with caster-based steering. The robot is equipped with independent wheel motors, an onboard computer, and a sensing suite including GNSS/IMU and a forward-facing camera. All algorithms are deployed through ROS2, enabling real-time control, data logging, and experimentation. The platform provides a reproducible environment for evaluating path following controllers and Bayesian-optimization-based parameter tuning. Fig. 1 presents an overview of the robot and illustrates the hardware configuration used in the experiments.

### B. Geometric Model

The AI-Formula robot uses its front wheel for both propulsion and steering, and the rear wheels do not contribute to the control inputs. Thus, the vehicle can be simplified as a non-holonomic two-wheel differential-drive mobile robot, as illustrated in Fig. 2.

In this mobile robot model,  $XOY$  denotes the world coordinate frame in the workspace. The target point is defined as a moving reference that includes its position, heading, and linear and angular velocities.  $O(x, y)$  represents the robot's center of gravity, located at the geometric midpoint between the left and right wheels,  $v$  the robot's linear velocity,  $\omega$  the robot's yaw rate,  $\phi$  the robot's global heading angle,  $O_t(x_t, y_t)$  the target's global position,  $v_t$  the target's linear velocity,  $\phi_t$  the target's global heading angle,  $\rho$  the distance between the robot and the target, and  $\theta_t$  the global angle from the robot's center  $O$  to target position  $O_t$ , respectively.

The robot's kinematics is described by

$$\dot{x} = v \cos \phi, \quad (1)$$

$$\dot{y} = v \sin \phi, \quad (2)$$

$$\dot{\phi} = \omega. \quad (3)$$

The relative positions and heading of the robot and the moving target point can be expressed as:

$$\rho \cos \theta_t = x_t - x, \quad (4)$$

$$\rho \sin \theta_t = y_t - y, \quad (5)$$

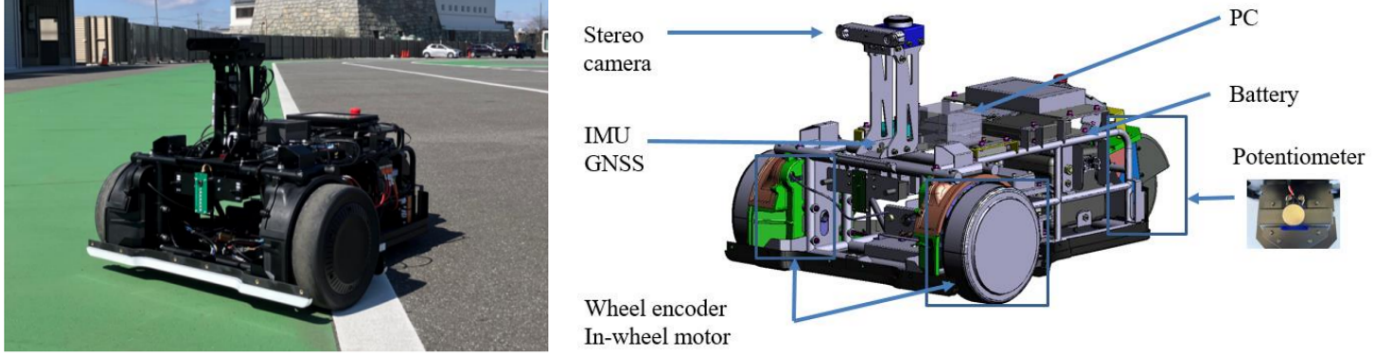


Fig. 1. Overall view and hardware configuration of the AI-Formula robot platform [30].

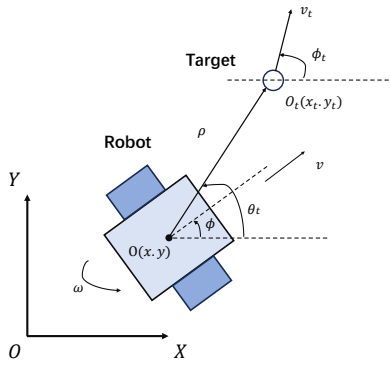


Fig. 2. Non-holonomic two-wheel differential-drive mobile robot model.

$$\alpha = \theta_t - \phi, \quad (6)$$

$$\beta = \phi_t - \phi. \quad (7)$$

$\alpha$  denotes the robot heading error, defined as the difference between  $\theta_t$  and the robot's heading  $\phi$ .  $\beta$  denotes the target heading misalignment error, defined as the difference between  $\theta_t$  and the target's heading  $\phi_t$ .

Their derivatives with respect to time  $t$  are:

$$\dot{\rho} = v_t \cos \beta - v \cos \alpha, \quad (8)$$

$$\dot{\alpha} = \frac{v \sin \alpha}{\rho} - \frac{v_t \sin \beta}{\rho} - \omega, \quad \rho \neq 0, \quad (9)$$

$$\dot{\beta} = \frac{v \sin \alpha}{\rho} - \frac{v_t \sin \beta}{\rho} - \dot{\phi}_t, \quad \rho \neq 0. \quad (10)$$

Note that the mobile robot model presented here is an idealized kinematic approximation. The implementation details are provided in the GitHub repository referenced in Section IV.

### C. Lyapunov Based Controller Design

In this work, the control objective is defined as tracking a moving target point. A Lyapunov-based geometric controller is designed to compute the linear velocity command  $v$  and angular velocity command  $\omega$  that stabilize the tracking error  $\rho$ ,  $\alpha$ , and  $\beta$ . The control law is obtained through the Lyapunov direct method. The Lyapunov function candidate is chosen as:

$$V = V_1 + V_2 \quad (11)$$

where

$$V_1 = \frac{1}{2} \rho^2, \quad (12)$$

$$V_2 = \frac{1 - \cos \alpha}{k_1} + \frac{1 - \cos \beta}{k_2}. \quad (13)$$

$k_1$  and  $k_2$  are the weighting constants.  $V_1$  quantifies the distance error  $\rho$ , and  $V_2$  quantifies the heading errors  $\alpha$  and  $\beta$ . Their sum forms a Lyapunov function that measures the overall tracking error of the system. Since  $V$  is positive definite, designing the control inputs such that  $\dot{V} \leq 0$  guarantees the convergence of both the position and orientation errors.

Differentiating  $V_1$  with respect to time  $t$  and substituting equation (8) for  $\dot{\rho}$  yields

$$\dot{V}_1 = \rho (v_t \cos \beta - v \cos \alpha). \quad (14)$$

The linear velocity input is designed as

$$v = (v_t \cos \beta + \lambda_v \rho) \cos \alpha, \quad (15)$$

with  $\lambda_v > 0$  a control gain. With this choice of  $v$ , the distance error  $\rho$  will converge toward zero when  $\alpha$  is sufficiently small.

*Proof.* Substituting equation (12) into  $\dot{V}_1$  gives

$$\dot{V}_1 = -\lambda_v \rho^2 \cos^2 \alpha + v_t \rho \sin^2 \alpha \cos \beta. \quad (16)$$

the first term is non-positive, while the second term is non-negative because  $v_t \geq 0$  and  $\sin^2 \alpha \geq 0$ . Since the positive term does not vanish unless  $\alpha \rightarrow 0$ ,  $\dot{V}_1$  cannot be non-positive in the general case. However, as  $\alpha \rightarrow 0$ , we have  $\sin^2 \alpha \rightarrow 0$  and  $\cos^2 \alpha \rightarrow 1$ , which causes the negative term to dominate,

$$\dot{V}_1 \rightarrow -\lambda_v \rho^2 < 0.$$

Thus,  $\dot{V}_1$  becomes negative semi-definite near the equilibrium, which satisfies the requirement of the Lyapunov direct method.  $\square$

Differentiating  $V_2$  with respect to time  $t$  and substituting equation (9), (10) and (15) yields

$$\begin{aligned} \dot{V}_2 = v_t & \left[ \frac{\sin^2 \alpha \cos \beta \cos \alpha}{k_1 \rho} - \frac{\sin \alpha \sin \beta}{k_1 \rho} \right. \\ & + \left. \frac{\sin \alpha \sin \beta \cos \beta \cos \alpha}{k_2 \rho} - \frac{\sin^2 \beta}{k_2 \rho} \right] \\ & + \lambda_v \cos \alpha \left( \frac{\sin^2 \alpha}{k_1} + \frac{\sin \alpha \sin \beta}{k_2} \right) \\ & - \frac{\sin \alpha}{k_1} \omega - \frac{\sin \beta}{k_2} \dot{\phi}_t. \end{aligned} \quad (17)$$

**Remark 1.** The expression of  $\dot{V}_2$  in [9] contains an algebraic error in the grouping of terms associated with  $v_t$ . The correct time derivative is derived here for consistency with the system dynamics.

The angular velocity input is designed as

$$\begin{aligned} \omega = \lambda_a \sin \alpha + \frac{k_1}{\sin \alpha} & \left\{ v_t \left[ \frac{\sin^2 \alpha \cos \beta \cos \alpha}{k_1 \rho} - \frac{\sin \alpha \sin \beta}{k_1 \rho} \right. \right. \\ & + \left. \left. \frac{\sin \alpha \sin \beta \cos \beta \cos \alpha}{k_2 \rho} - \frac{\sin^2 \beta}{k_2 \rho} \right] \right. \\ & \left. + \lambda_v \cos \alpha \left( \frac{\sin^2 \alpha}{k_1} + \frac{\sin \alpha \sin \beta}{k_2} \right) \right\} - \frac{k_1 \sin \beta}{k_2 \sin \alpha} \dot{\phi}_t. \end{aligned} \quad (18)$$

with  $\lambda_a > 0$  a control gain. With this choice of  $\omega$ , the heading error  $\alpha$  and  $\beta$  will converge toward zero. As  $\alpha \rightarrow 0$ , the positive term in  $\dot{V}_1$  vanishes, ensuring that  $\dot{V}_1 < 0$  and thus  $\rho \rightarrow 0$ .

*Proof.* Substituting the angular velocity input into the expression of  $\dot{V}_2$  yields

$$\dot{V}_2 = -\frac{\lambda_a}{k_1} \sin^2 \alpha \leq 0. \quad (19)$$

All terms in  $\dot{V}_2$  except  $-\frac{\lambda_a}{k_1} \sin^2 \alpha$  are canceled by the designed control input  $\omega$ . Since  $\lambda_a > 0$  and  $\sin^2 \alpha \geq 0$ , the  $\dot{V}_2$  is negative semi-definite, which implies that the heading error  $\alpha$  and  $\beta$  converges to zero according to the Lyapunov direct method.  $\square$

In summary, the Lyapunov-based geometric controller is completed by the linear velocity input in (15) together with the angular velocity input in (18), ensuring the convergence of both position and heading errors.

**Remark 2.** All four gains  $(\lambda_v, \lambda_a, k_1, k_2)$  contribute to the expression of  $\dot{V}_2$  through nonlinear and coupled terms that involve products or ratios with the state variables. Consequently, modifying any single gain influences multiple components of the Lyapunov derivatives, making it impossible to tune their effects on the closed-loop behavior independently. In practice, this coupling structure makes the manual tuning problem of  $(\lambda_v, \lambda_a, k_1, k_2)$  into a time-wasting trial-and-error process in a four-dimensional parameter space, where obtaining a

balanced trade-off between stability and tracking accuracy often requires numerous real-vehicle experiments. These observations highlight the need for a data-efficient automatic tuning method capable of exploring such coupled parameter interactions with a limited number of evaluations. As a result, we employ Bayesian optimization to perform a systematic and sample-efficient search over the parameter space, enabling effective tuning under the real-world experiment conditions.

#### D. Parameter Tuning Problem

In this subsection we formalize the controller tuning problem addressed in this work. The controller presented in subsection II-C depends on five tunable parameters  $\{v_t, \lambda_v, \lambda_a, k_1, k_2\}$ , where the target velocity  $v_t$  is fixed during operation. Therefore, the tuning task focuses on the four controller gains  $\{\lambda_v, \lambda_a, k_1, k_2\}$ . The Integral of Absolute Error (IAE) provides a standard way to quantify tracking performance as the accumulated deviation over time [31]:

$$\text{IAE} = \int_0^\infty |y_r(t) - y(t)| dt = \sum_{k=0}^K |y_r(k) - y(k)| \Delta t, \quad (20)$$

where  $y_r(t)$  and  $y(t)$  denote the reference and measured outputs, respectively,  $K$  is the last time step in the recording horizon for discrete system, and  $\Delta t$  is the sampling interval.

In this work, the performance is evaluated from real vehicle experiments by quantifying the lateral deviation from the reference path and the heading misalignment with respect to the reference heading. Accordingly, the performance function  $J_{\text{sum}}$  combines both lateral and heading tracking errors. To avoid scale imbalance between the two error components, each term is normalized by its median magnitude, ensuring that the optimization does not become biased. Moreover, a weighting factor is employed to tune the relative contribution of each error term within the cost function. Thus,  $J_{\text{sum}}$  is defined as:

$$J = J_{\text{lat}} + w \cdot J_{\text{head}}, \quad w > 0, \quad (21)$$

where

$$J_{\text{lat}} = \frac{\sum_{k=0}^K |e_{\text{lat}}(k)|}{\text{median}(|e_{\text{lat}}|)}, \quad (22)$$

$$J_{\text{head}} = \frac{\sum_{k=0}^K |e_{\text{head}}(k)|}{\text{median}(|e_{\text{head}}|)}. \quad (23)$$

$e_{\text{lat}}(k)$  and  $e_{\text{head}}(k)$  represent the lateral tracking error and heading error at time step  $k$ , and  $w > 0$  is the weighting coefficient.

In this way, the tuning problem can be summarized as the following black-box optimization problem:

$$\begin{aligned} & \min_{\theta \in \Theta} J(\theta), \\ \text{s.t.} \quad & \theta = [\lambda_v, \lambda_a, k_1, k_2]^\top, \\ & \lambda_v, \lambda_a, k_1, k_2 \in \mathbb{R}^+, \\ & \Theta = \left\{ \theta \mid \theta^{\text{lb}} \leq \theta \leq \theta^{\text{ub}} \right\}. \end{aligned} \quad (24)$$

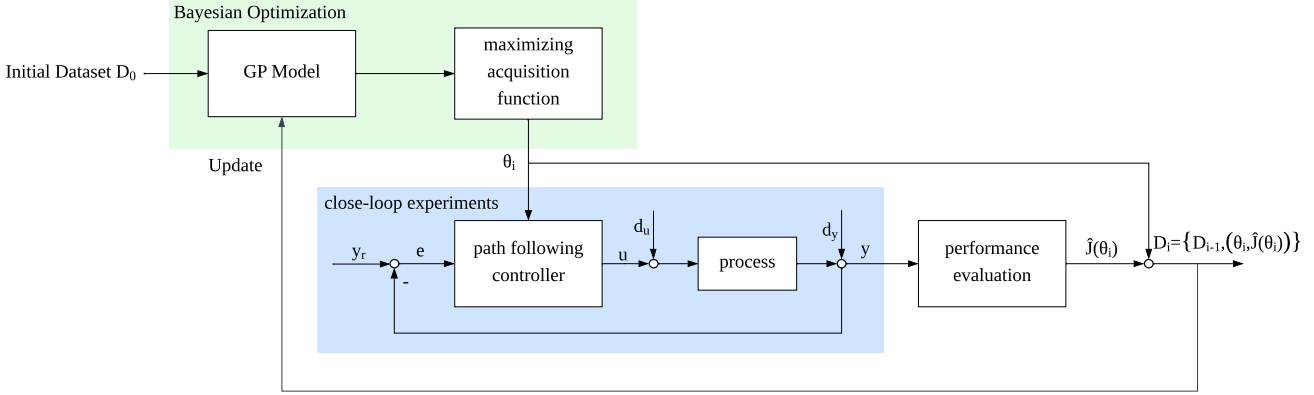


Fig. 3. Overview of the proposed BO framework for path following controller tuning. The acquisition function selects a parameter vector  $\theta_i$ , which is applied to the closed-loop experiment (blue region). The path-following controller uses the reference  $y_r$  and the tracking error  $e$  to generate the control input  $u$ , while actuator disturbances  $d_u$  and measurement disturbances  $d_y$  affect the process and its measured output  $y$ . After completing an entire run, the performance evaluation block gives the noisy performance evaluation  $\hat{J}(\theta_i)$ , which is appended to the dataset  $D_i = \{D_{i-1}, (\theta_i, \hat{J}(\theta_i))\}$ . The augmented dataset is then used to update the Gaussian process (GP) surrogate model and BO selects the next gain vector  $\theta_{i+1}$  via the acquisition function. In this way, an iterative outer-loop optimization is established, with BO repeatedly guiding successive closed-loop experiments.

Here,  $\theta$  denotes the tested gain vector,  $\theta^{\text{lb}}$  and  $\theta^{\text{ub}}$  denote the lower and upper admissible bound vectors for the controller gain vector  $\theta$ , respectively. These bounds confine the BO search to safe and feasible regions for real-world operation. Moreover, the controller used in this study has been validated in real-world experiments [32]. The experiment results demonstrate that the controller maintains consistently stable and reliable closed-loop behavior under practical operating conditions.

Table I summarizes the fixed experimental settings and the parameter-domain specifications used throughout the BO tuning process. These include the reference tracking conditions, BO loop configuration, penalization coefficient, and the lower-upper bounds that define the admissible search region  $\Theta$  for the controller gains. All values remain unchanged for every experiment reported in Section IV.

### III. PROPOSED BAYESIAN OPTIMIZATION FRAMEWORK

#### A. Overview of the BO Tuning Loop

In this section, the tuning of the controller gains is formulated as a data-driven experimental optimization problem, since the performance index  $J(\theta)$  cannot be computed analytically and is only available through closed-loop experiments. In this context, BO is well suited for the tuning task because (i) its high sample efficiency is essential when each experiment requires a full closed-loop run; (ii) its probabilistic surrogate explicitly represents uncertainty and improves robustness against measurement noise; (iii) it does not rely on gradients or smoothness, which aligns with the black-box nature of real-world experiments. The schematic structure of the proposed BO based tuning framework is illustrated in Fig. 3.

#### B. Gaussian Process Surrogate

In BO, a surrogate model captures the relationship between controller gains and performance by approximating  $J(\theta)$  in

untested regions, thereby guiding the selection of new evaluations. In this work, we adopt a GP surrogate to model the mapping of  $J(\theta)$  over the parameter space with predictive mean and variance. Compared with surrogate models that provide only point predictions, GP models the joint statistical structure across all parameter values, allowing BO to update the entire model with each new observation [33], [34].

As illustrated in Section II-D, the closed-loop performance index is modeled as an unknown function  $J : \Theta \rightarrow \mathbb{R}, \Theta \subset \mathbb{R}^4$ , and the tuning task aims at finding

$$\theta^* = \arg \min_{\theta \in \Theta} J(\theta). \quad (25)$$

To model the unknown structure of  $J(\theta)$  over the high-dimensional parameter space, we assign the GP prior as:

$$J(\theta) \sim \mathcal{GP}(m(\theta), k(\theta, \theta')), \quad (26)$$

where the mean function  $m(\theta)$  represents the prior expectations of the tested gain vector  $\theta$ , and the covariance kernel  $k(\theta, \theta')$  represents the correlation structure of the surrogate. The GP prior thus enables Bayesian optimization to combine prior knowledge with experimental data in a principled manner, producing prediction that guide the exploration as well as the exploitation during the tuning process. We use an ARD Matérn-5/2 kernel for  $k(\theta, \theta')$ , which assigns different length-scales to each gain dimension and thereby captures the anisotropic structure of the parameter space. Additionally, the Matérn-5/2 kernel provides moderate non-smooth behavior that matches real experimental data with disturbance while keeping the surrogate sufficiently smooth for stable prediction [35].

In the  $i$ -th real-world experiment, the closed-loop system is operated with the gain vector  $\theta_i$ , and the resulting noisy performance evaluation is

$$\hat{J}(\theta_i) = J(\theta_i) + \varepsilon_i, \quad \varepsilon_i \sim \mathcal{N}(0, \sigma_n^2), \quad (27)$$

where  $\widehat{J}(\boldsymbol{\theta}_i)$  is the noisy measured performance index, and  $J(\boldsymbol{\theta})$  denotes the true performance function value (noise-free). The noise term  $\varepsilon_i$  aggregates all experimental disturbances, including the actuator disturbance  $d_u$ , the output disturbance  $d_y$ , sensor noise, and the residual variations arising from the inherent non-repeatability of real-world vehicle experiments.

Under the GP prior, the noisy evaluations at the first  $i$  sampled parameter vectors and the evaluation at a new parameter  $\boldsymbol{\theta}_{i+1}$  follow a joint Gaussian distribution, which can be written as:

$$\begin{bmatrix} \widehat{\mathbf{J}}_{1:i} \\ J(\boldsymbol{\theta}_{i+1}) \end{bmatrix} \sim \mathcal{N}\left(\begin{bmatrix} \mathbf{m}_{1:i} \\ m(\boldsymbol{\theta}_{i+1}) \end{bmatrix}, \begin{bmatrix} K_i + \sigma_n^2 I & k_i(\boldsymbol{\theta}_{i+1}) \\ k_i(\boldsymbol{\theta}_{i+1})^\top & k(\boldsymbol{\theta}_{i+1}, \boldsymbol{\theta}_{i+1}) \end{bmatrix}\right), \quad (28)$$

where the vectors of noisy evaluations and prior means are

$$\widehat{\mathbf{J}}_{1:i} = \begin{bmatrix} \widehat{J}(\boldsymbol{\theta}_1) \\ \vdots \\ \widehat{J}(\boldsymbol{\theta}_i) \end{bmatrix}, \quad \mathbf{m}_{1:i} = \begin{bmatrix} m(\boldsymbol{\theta}_1) \\ \vdots \\ m(\boldsymbol{\theta}_i) \end{bmatrix}, \quad (29)$$

and the covariance terms are given by

$$K_i = \begin{bmatrix} k(\boldsymbol{\theta}_1, \boldsymbol{\theta}_1) & \cdots & k(\boldsymbol{\theta}_1, \boldsymbol{\theta}_i) \\ \vdots & \ddots & \vdots \\ k(\boldsymbol{\theta}_i, \boldsymbol{\theta}_1) & \cdots & k(\boldsymbol{\theta}_i, \boldsymbol{\theta}_i) \end{bmatrix}, \quad (30)$$

$$k_i(\boldsymbol{\theta}_{i+1}) = \begin{bmatrix} k(\boldsymbol{\theta}_1, \boldsymbol{\theta}_{i+1}) \\ \vdots \\ k(\boldsymbol{\theta}_i, \boldsymbol{\theta}_{i+1}) \end{bmatrix}. \quad (31)$$

Given the joint Gaussian model in (28), conditioning on the  $i$  observed evaluations amounts to conditioning on the dataset  $D_i = \{(\boldsymbol{\theta}_j, \widehat{J}(\boldsymbol{\theta}_j))\}_{j=1}^i$ . For any test candidate  $\boldsymbol{\theta}$ , the resulting GP posterior distribution of the true value  $J(\boldsymbol{\theta})$  is

$$J(\boldsymbol{\theta}) \mid D_i \sim \mathcal{N}(\mu_i(\boldsymbol{\theta}), \sigma_i^2(\boldsymbol{\theta})), \quad (32)$$

with posterior mean

$$\mu_i(\boldsymbol{\theta}) = m(\boldsymbol{\theta}) + k_i(\boldsymbol{\theta})^\top (K_i + \sigma_n^2 I)^{-1} (\widehat{\mathbf{J}}_{1:i} - \mathbf{m}_{1:i}), \quad (33)$$

and posterior variance

$$\sigma_i^2(\boldsymbol{\theta}) = k(\boldsymbol{\theta}, \boldsymbol{\theta}) - k_i(\boldsymbol{\theta})^\top (K_i + \sigma_n^2 I)^{-1} k_i(\boldsymbol{\theta}). \quad (34)$$

Note that the prior mean can be set to  $m(\boldsymbol{\theta}) = 0$ , which is the standard assumption when no prior trend of the function is known. In GP regression, the mean function represents only a constant offset, and this offset is automatically cancelled once data are conditioned on. Therefore, using a zero prior mean does not affect how the model fits the underlying function.

The remaining unspecified components of the GP are the hyperparameters of the covariance function together with the noise variance  $\sigma_n^2$ . These hyperparameters determine the correlation structure of the function over the parameter space. Their values are determined by maximizing the marginal log-likelihood of the observed data, following standard GP practice [36].

The remaining unspecified components of the GP are the hyperparameters  $\phi$ , which include the parameters of the covariance kernel (e.g. length scales and signal variance) as well as the noise variance  $\sigma_n^2$ . These hyperparameters determine the

smoothness and correlation structure of the surrogate model over the parameter space. Following standard GP practice [36], their values can be obtained by maximizing the marginal log-likelihood of the observed data:

$$\phi^* = \arg \max_{\phi} \log p(\widehat{\mathbf{J}}_{1:i} \mid \phi). \quad (35)$$

### C. Acquisition Function and Selection of the Next Evaluation Point

Given the GP posterior established in the previous subsection, Bayesian optimization evaluates candidate gain vectors through their posterior mean  $\mu_i(\boldsymbol{\theta})$  and variance  $\sigma_i^2(\boldsymbol{\theta})$ . These posterior parameters reflect both the predicted performance and the uncertainty of that prediction. To convert this information into a decision rule for selecting the next experiment, an acquisition function is introduced.

The acquisition function provides a principled rule for guiding the selection of the next evaluation point, replacing ad-hoc or heuristic search strategies with a statistically grounded decision mechanism. In this study, we employ the Expected Improvement (EI) as the acquisition function, guiding the search toward parameter candidates with the greatest improvement potential.

Let the best observed performance after  $i$  experiments be

$$J_{\min}^{(i)} = \min_{1 \leq j \leq i} \widehat{J}(\boldsymbol{\theta}_j). \quad (36)$$

For any potential optimum candidate  $\boldsymbol{\theta}$ , the improvement over the current best is defined as

$$I(\boldsymbol{\theta}) = \max(J_{\min}^{(i)} - J(\boldsymbol{\theta}), 0), \quad (37)$$

and the corresponding expected improvement under the GP posterior (32) is

$$\begin{aligned} EI_i(\boldsymbol{\theta}) &= (J_{\min}^{(i)} - \mu_i(\boldsymbol{\theta})) \Phi\left(\frac{J_{\min}^{(i)} - \mu_i(\boldsymbol{\theta})}{\sigma_i(\boldsymbol{\theta})}\right) \\ &\quad + \sigma_i(\boldsymbol{\theta}) \phi\left(\frac{J_{\min}^{(i)} - \mu_i(\boldsymbol{\theta})}{\sigma_i(\boldsymbol{\theta})}\right), \end{aligned} \quad (38)$$

where  $\mu_i(\boldsymbol{\theta})$  and  $\sigma_i(\boldsymbol{\theta})$  denote the GP posterior mean and standard deviation, and  $\Phi(\cdot)$  and  $\phi(\cdot)$  are the standard normal cumulative distribution function (CDF) and probability density function (PDF), respectively. The CDF term, driven by  $(J_{\min}^{(i)} - \mu_i(\boldsymbol{\theta}))$ , guides exploitation toward candidates with promising predicted performance, whereas the PDF term, scaled by  $\sigma_i(\boldsymbol{\theta})$ , guides exploration toward regions with high model uncertainty. Together, these two components allow EI to balance improving the current best solution with exploring regions where uncertainty remains high. With the acquisition function established, the overall BO tuning procedure for  $N_{\max}$  experiments is summarized in Algorithm 1.

**Algorithm 1** BO Loop for Controller Parameter Tuning

- 1: **Input:** parameter domain  $\Theta$ , GP prior on  $J(\theta)$ , acquisition function  $\alpha_i(\theta)$  (EI)
- 2: **Initialization:** choose  $N_{\text{init}}$  initial gains  $\{\theta_j\}_{j=1}^{N_{\text{init}}} \subset \Theta$  and run closed-loop experiments to obtain initial dataset  $D_{N_{\text{init}}} = \{(\theta_j, \hat{J}(\theta_j))\}_{j=1}^{N_{\text{init}}}$
- 3: **for**  $i = N_{\text{init}}, \dots, N_{\text{max}} - 1$  **do**
- 4:   Update GP posterior  $(\mu_i(\theta), \sigma_i^2(\theta))$  using  $D_i$
- 5:   Optionally update the hyperparameters  $\phi$  by maximizing the marginal log-likelihood of  $D_i$  (not necessarily at every iteration).
- 6:   Select next gain vector  $\theta_{i+1} = \arg \max_{\theta \in \Theta} \text{EI}_i(\theta)$
- 7:   Apply  $\theta_{i+1}$  in the real-vehicle closed-loop experiment and measure  $\hat{J}(\theta_{i+1})$
- 8:   Update dataset  $D_{i+1} = D_i \cup \{(\theta_{i+1}, \hat{J}(\theta_{i+1}))\}$
- 9: **end for**
- 10: **Output:**  $\theta^* = \arg \min_{(\theta_j, \hat{J}(\theta_j)) \in D_{N_{\text{max}}}} \hat{J}(\theta_j)$

**D. Implementation of BO on the AI-Formula Robot**

The BO framework described above is applied on Honda's AI-Formula robot introduced in Section II-A. In contrast to simulation studies, each evaluation of  $J(\theta)$  requires a full real-vehicle lap under closed-loop control, carried out on a fixed reference path and target speed. Real-world experiments are affected by measurement noise, model mismatch, run-to-run variability, and hardware limits, which make direct application of standard BO not sufficient. To enhance the evaluation efficiency, the tuning framework must be customized. In this subsection, we detail the modifications used to implement BO on the AI-Formula robot.

*Initial data collection:* A Bayesian optimization loop can be started without prior evaluations, but doing so is inadvisable for real-world experiments where the experiment budget is limited. To provide initial evaluations with adequate coverage of the parameter space, we construct an initial dataset  $D_{\text{init}} = \{(\theta_j, \hat{J}(\theta_j))\}_{j=1}^{N_{\text{init}}}$ , comprised of the manual baseline gain vector together with additional samples generated based on space filling over the feasible parameter region. This warm-start initialization substantially accelerates convergence by allowing the surrogate model to start with informative structure rather than relying on blind exploration during the early BO iterations, thereby guiding the search more efficiently toward a sufficiently good solution.

*Logarithmic specification of gain ranges:* The four controller gains affect the closed-loop behaviour at very different numerical ranges, so their meaningful values do not lie on a common linear scale. Defining the search domain directly in the linear space would therefore place most candidates in regions with negligible impact on the system response.

Therefore, to obtain a more balanced coverage of the search space, the feasible domain as well as the initial sampling of each gain should be defined in the logarithmic scale. Additionally, for each gain  $\theta_k$  ( $k = 1, \dots, 4$ ), we introduce the transformed variable  $z_k = \log(\theta_k)$ , and BO is carried out in the  $z_k$  space. The controller gains used in the experiments are recovered through  $\theta_k = \exp(z_k)$ . This formulation allows



Fig. 4. Overview of the real-world test course.

BO to account for the different scales of the gains and prevents the loss of resolution inherent in a linear scaling.

*Safety handling and penalization strategy:* A small fraction of gain combinations inevitably produce unstable closed-loop responses on the real vehicle. Rather than discarding these trials, their outcomes are encoded using a finite penalty value. This marks the corresponding region of the parameter space as unfavorable, discouraging BO from sampling in its neighborhood while still allowing points that are sufficiently distant from the instability boundary to be explored.

*Stopping criteria:* The BO loop operates under a finite experimental budget, so the number of closed-loop evaluations is capped at  $N_{\text{max}}$ . Beyond this limit, the optimization may also terminate early when the acquisition function suggests that additional evaluations are unlikely to yield improvement. In practice, the loop is stopped once the maximum Expected Improvement (EI) falls below a small threshold or when the best observed performance  $J_{\min}^{(i)}$  has stabilized over several consecutive iterations.

## IV. REAL-WORLD EXPERIMENTS AND RESULTS

This section presents the real-world experiments used to evaluate the proposed BO-based gain-tuning framework and reports the resulting performance on the AI-Formula robot. All software components used in the experiments are implemented in ROS2 and made publicly available in the project repository [https://github.com/SophiaControl/AIformula\\_sophia](https://github.com/SophiaControl/AIformula_sophia).

### A. Experimental Setup

In this work, the real-world experiments are conducted on the AI-Formula robot introduced in Section II-A. All evaluations of  $J(\theta)$  are performed on a fixed test track at Honda's vehicle test course, shown in Fig. 4. A reference trajectory is defined on this track and kept unchanged throughout all experiments. Each BO evaluation corresponds to one complete lap of this trajectory under closed-loop control at a fixed target speed. By keeping the trajectory and operating conditions

fixed, the observed performance variations reflect mainly the effect of the controller gains.

In the experiments, the performance index follows the formulation introduced in Section II-D, where the lap-based tracking cost  $J_{\text{sum}}(\theta)$  combines the lateral and heading errors along the fixed reference trajectory. Closed-loop instability is handled through the penalization mechanism described in Section III-D, which allows incomplete laps to be retained in a consistent way within the BO dataset.

The scalar value actually returned to the BO loop is defined as

$$\hat{J}_{\text{BO}}(\theta) = \hat{J}(\theta) + \lambda_{\text{pen}} \left( 1 - \frac{L_{\text{comp}}}{L_{\text{lap}}} \right), \quad (39)$$

where  $L_{\text{comp}}$  is the distance completed before loss of closed-loop stability,  $L_{\text{lap}}$  is the full lap length, and  $\lambda_{\text{pen}} > 0$  is a finite penalty weight. For stable trials one has  $L_{\text{comp}} = L_{\text{lap}}$  and hence  $\hat{J}_{\text{BO}}(\theta) = \hat{J}(\theta)$ , whereas unstable runs receive a larger  $\hat{J}_{\text{BO}}(\theta)$ , which naturally keep BO away from gain regions that cause divergence while still preserving the information that such settings were tested.

The experiments were conducted under repeatable operating conditions, with identical sensor configuration, control frequency, and environment, so that variations in performance can be attributed solely to the controller gains.

Table I illustrates the fixed experimental settings and the parameter-domain specifications used throughout the BO tuning process. These include the reference tracking conditions, BO loop configuration, penalization coefficient, and the lower-upper bounds that define the admissible search region  $\Theta$  for the controller gains. All values remain unchanged for every experiment reported in Section IV.

TABLE I  
EXPERIMENTAL SETTINGS AND BO PARAMETER-DOMAIN SPECIFICATION

| Variable                                 | Value  | Meaning              |
|--|--|----------------------|
| $v_t$                                    | 2 m/s  | Reference velocity   |
| $w$                                      | 0.1  | Weighting factor     |
| $N_{\text{init}}$                        | 15   | Initial sample size  |
| $N_{\text{max}}$                         | 32   | BO evaluation budget |
| $\lambda_{\text{pen}}$                   | 7000   | Penalty coefficient  |
| <b>Search domain <math>\Theta</math></b> | $\{\theta \mid \theta^{\text{lb}} \leq \theta \leq \theta^{\text{ub}}\}$ |                      |
| $\lambda_v$                              | $[10^{-4}, 0.5]$   |                      |
| $\lambda_a$                              | $[10^{-3}, 1.5]$   |                      |
| $k_1$                                    | $[10^{-2}, 10]$  |                      |
| $k_2$                                    | $[10^{-1}, 100]$   |                      |

## B. Experiment Result and Discussion

For each BO iteration, the selected gain vector  $\theta_i$  is applied to the Lyapunov-based controller on Honda's AI-Formula robot. Starting from the crosswalk section of the test track shown in Fig. 4, the vehicle follows a fixed reference trajectory for one complete counterclockwise lap under closed-loop control. At the end of the lap, the performance index is evaluated according to (39), yielding the scalar value  $\hat{J}_{\text{BO}}(\theta_i)$ , which is returned to the BO loop as the observation used to update the GP surrogate.

To ensure experimental repeatability, all trials are executed under identical sensor configurations and control settings. The path-following controller runs at 100 Hz, and vehicle states are logged at 10 Hz for evaluating the performance index. Each BO evaluation begins from the same initial pose on the track with the vehicle aligned to the reference direction and accelerated to the fixed target speed before the cost accumulation starts. Although this procedure minimizes initial-condition variability, invisible disturbance like the passive rear wheel's heading can introduce unavoidable run-to-run disturbances, which contribute to the measurement noise in real-world experiments.

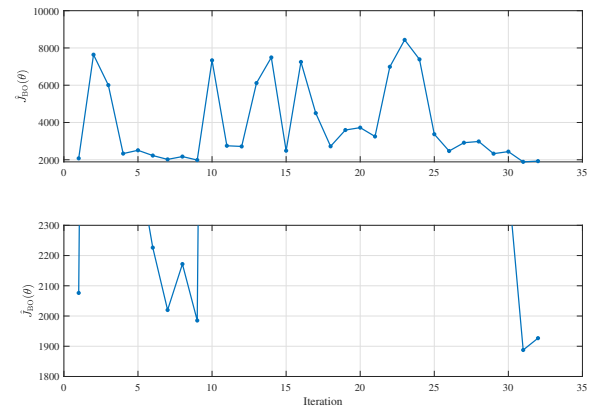


Fig. 5. Experimentally evaluated performance  $\hat{J}_{\text{BO}}(\theta)$  over iterations

Fig. 5 shows the experimentally evaluated performance  $\hat{J}_{\text{BO}}(\theta)$  over the BO iterations. The upper plot displays all evaluations across the full cost range, while the lower plot zooms in on the neighborhood of the best values to make the convergence trend more visible.

*a) Iterations 1–15:* The first BO iteration corresponds to the manually tuned baseline gain vector described in Section III-D. This baseline was originally obtained in [32] through an extensive trial-and-error process informed by the simulation study of [9]. In that process, each of the four controller gains was tuned individually within the neighborhood of the parameter values suggested by [9], and approximately forty real-world trials were conducted to identify a combination that produced consistently stable and acceptable closed-loop tracking behavior on the AI-Formula platform. This procedure yielded a practically satisfactory setting,  $\{\lambda_v, \lambda_a, k_1, k_2\} = \{0.02, 0.25, 0.7, 50\}$ , which produced a performance value of  $\hat{J}_{\text{BO}} = 2076.35$  when evaluated using (39). Although manual tuning can provide reasonably good tracking behavior, it is ultimately the product of a time-consuming manual search rather than a systematic optimization process. Under the limited experimental budget available in real-vehicle testing, such exploration becomes highly constrained. It is infeasible to systematically explore the broader parameter space, especially when the controller contains multiple strongly coupled gains. As a result, the search process remains largely blind to global structure, and the chance of encountering near-optimal settings depends more on luck than on informed exploration, since a

comprehensive understanding of the full gain landscape cannot be built from a small number of noisy closed-loop trials.

Iterations 2–15 constitute the remaining initial dataset ( $N_{\text{init}} = 15$ ) used to warm-start the BO loop. These gain vectors were generated through a hybrid space-filling strategy: Iterations 2–7 sample the neighbourhood of the manually tuned baseline, while Iterations 8–15 distribute points more broadly across the feasible domain. This design provides both local refinement around a known workable region and global coverage of the wider gain space.

The resulting performance values span a large range, including several unstable trials ( $\hat{J}_{\text{BO}} > 3000$ ), which provide useful information about unsafe regions. Although Iterations 2 and 3 lie close to the baseline in parameter space, they still result in instability, illustrating the sensitivity and coupling of the gains. In contrast, Iterations 4–7 remain stable and deliver performances only slightly worse than the baseline, with Iteration 7  $\{\lambda_v, \lambda_a, k_1, k_2\} = \{0.0220, 0.2200, 0.7500, 48\}$ ,  $\hat{J}_{\text{BO}} = 2019.88$ , already marginally outperforming the manually tuned baseline. Iterations 8–15 explore regions farther from the baseline; some yield divergence, while others such as Iteration 9  $\{\lambda_v, \lambda_a, k_1, k_2\} = \{0.017, 0.23, 0.8, 40\}$ ,  $\hat{J}_{\text{BO}} = 1985.14$ , demonstrating that superior performance can be found outside the manually selected neighbourhood. This hybrid space-filling strategy essentially behaves like a randomized search with a very limited number of samples. With only 14 additional trials, the initial set cannot cover the gain space densely, but the mixture of stable and unstable outcomes in iterations 1–15 still provides heterogeneous information for constructing the initial GP surrogate.

*b) Iterations 16–32:* After the initial warm-start phase, the BO loop proceeds with sequential acquisition-driven evaluations. A clear transition occurs at the beginning of this stage. Iteration 16 yields a penalized cost of  $J_{\text{BO}} = 7248.79$ , far exceeding all previous stable evaluations and indicating that the closed-loop system became unstable shortly after the start of the lap. The corresponding gain vector,  $\{\lambda_v, \lambda_a, k_1, k_2\} = \{0.001496, 0.0035065, 0.12699, 99.746\}$ , lies in a region that was still poorly informed by the initial data. This indicates that, in the early phase, the surrogate guides exploration into regions whose safety cannot yet be reliably assessed due to limited model certainty.

In the following stage (Iterations 17–24), the BO loop remains exploration-dominated. The surrogate model is still adapting to the high dimensional parameter landscape, and its uncertainty leads the acquisition function to propose gain vectors in regions whose stability cannot yet be reliably assessed. As a result, the penalized costs in this interval remain large, and unstable behavior occurs frequently. Even the stable trials in this phase generally yield high costs, indicating that the search has not yet converged toward any consistently well-performing region. This behavior is consistent with the expected early dynamics of BO, where broad exploration is required before meaningful exploitation can take place.

Once sufficient information has been gathered, the sampling pattern begins to shift. Starting around Iteration 25, the evaluations become more stable and the cost values progressively

decrease. A clear convergence trend emerges across Iterations 25–32, during which the BO loop repeatedly samples within a region that offers substantially improved closed-loop performance relative to earlier trials.

Among all evaluations, Iteration 31 attains the lowest cost,  $\hat{J}_{\text{BO}} = 1887.65$ ,  $\{\lambda_v, \lambda_a, k_1, k_2\} = \{0.014, 0.29, 0.70, 48\}$ , representing the best performance observed over the entire experiment set. Iteration 32 produces a similarly competitive outcome:  $\hat{J}_{\text{BO}} = 1926.77$ ,  $\{\lambda_v, \lambda_a, k_1, k_2\} = \{0.016, 0.27, 0.72, 45\}$ , and both results outperform the manually tuned baseline (2076.35). These observations confirm that BO successfully identifies high-performing gain configurations within the limited real-vehicle evaluation budget.

In addition, real-world experiments are affected by considerable measurement noise. Each closed-loop lap lasts several minutes, during which the evaluated performance is influenced by sensor drift, actuator imperfections, and varying environmental conditions. These disturbances can cause the measured value of  $\hat{J}_{\text{BO}}(\theta)$  to deviate from the true performance. Such disturbances can misrank gain vectors, making suboptimal settings appear competitive or penalizing genuinely good ones. With limited experimental budget, these misjudgements cannot be corrected through repeated trials and may steer the search toward uninformative regions of the gain space. Consequently, the overall performance landscape cannot be reliably inferred from a limited number of noisy evaluations, rendering manual tuning ineffective.

These difficulties underscore the need for an optimization method that can work with noisy measurements and limited trials. Bayesian optimization provides this capability by systematically balancing exploration and exploitation, making it well suited for tuning the coupled gains of the controller.

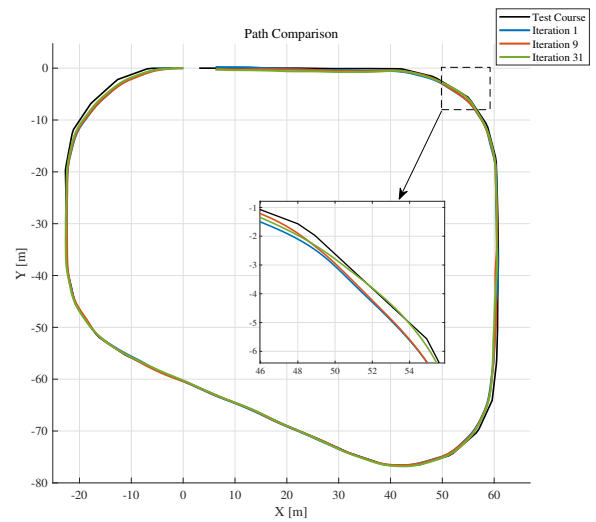


Fig. 6. Path comparison across selected BO iterations. The plot shows the reference test course together with the closed-loop trajectories obtained at Iterations 1 (manual baseline), 9 (early improvement within the initial space-filling set), and 31 (best-performing BO result).

To illustrate how parameter updates influence the closed-loop behaviour, Fig. 6 compares the trajectories obtained at three representative iterations. Iteration 1 corresponds to

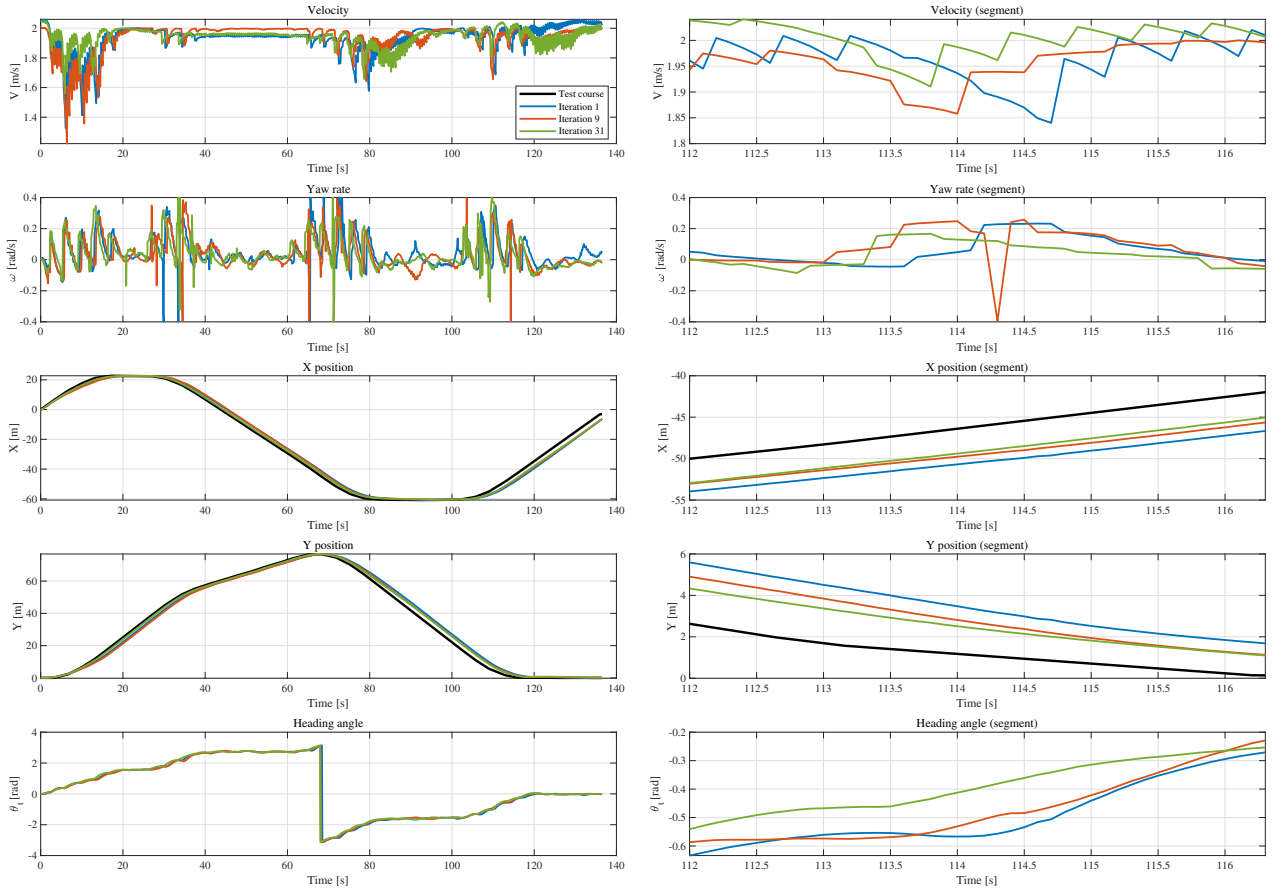


Fig. 7. State trajectories for Iterations 1, 9 and 31 along the normalized path progress. The left column shows the full-lap profiles of velocity, yaw rate, global  $x$  and  $y$  position, and heading angle. The right column presents zoomed views of the same quantities over the corner segment indicated in Fig. 6.

the manually tuned baseline described earlier. Iteration 9 represents the best-performing sample within the initial space-filling evaluations, already showing noticeable improvement over the baseline. Iteration 31 is the best result produced by BO, yielding the lowest cost in all 32 experiments. Across these three trajectories, the improvement in tracking accuracy is most visible in the curved sections of the course, where the BO tuned gains reduce overshoot and lateral deviation with respect to the reference path.

A more detailed comparison of the vehicle states for Iterations 1, 9 and 31 is given in Fig. 7, where velocity, yaw rate, position and heading are plotted as functions of time, together with zoomed views of the segment highlighted in Fig. 6. In the velocity plots, the manually tuned baseline (Iteration 1) exhibits larger fluctuations and several noticeable dips along the lap, especially near the corner segment. Iteration 9 already reduces part of this variability, while the BO tuned setting at Iteration 31 produces the smoothest speed profile, remaining closest to the nominal target velocity. A similar trend is observed in the yaw rate. The baseline shows sharper peaks and more pronounced oscillations, indicating stronger corrective steering actions. Iteration 9 moderates these peaks, and Iteration 31 further suppresses unnecessary yaw rate excursions in the zoomed segment.

The  $x$  and  $y$  position traces confirm the conclusions drawn

TABLE II  
LATERAL ERROR AND HEADING ERRORS FOR ITERATIONS 1, 9, AND 31

| Iteration | Lateral error (m) |       |       | Heading error (deg) |       |        |
|-----------|-------------------|-------|-------|---------------------|-------|--------|
|           | Mean              | RMS   | Max   | Mean                | RMS   | Max    |
| 1         | 0.424             | 0.478 | 1.130 | 2.594               | 3.721 | 18.808 |
| 9         | 0.422             | 0.477 | 1.152 | 2.667               | 3.813 | 18.443 |
| 31        | 0.415             | 0.459 | 0.927 | 2.672               | 3.714 | 17.389 |

from the path comparison. Over the full lap the three experiments follow the same general course, but in the zoomed view the Iteration 31 trajectory stays closest to the reference in both coordinates. The heading angle plot shows that the BO tuned controller also achieves a smoother change of orientation in the curved section, reducing overshoot relative to the baseline Iteration 1 and the Iteration 9 setting. Together, these results illustrate how the BO procedure translates improved values of  $\hat{J}_{BO}$  into visibly better state trajectories on the AI-formula robot.

Table II compares the lateral and heading errors for Iterations 1, 9, and 31. The results for Iterations 1 and 9 are nearly identical, indicating that the manually tuned baseline already provides reasonably good performance. In comparison, Iteration 31 shows measurable improvements. The maximum lateral error decreases from roughly 1.13–1.15 m to 0.93 m,

corresponding to a reduction of about 18%, and the RMS lateral error drops by approximately 4%. The maximum heading error is reduced by around 7%, yielding the smallest overall heading excursions among the three iterations. These reductions reflect a more consistent tracking behaviour, particularly in curved segments of the track where lateral accumulation effects are most pronounced. While the numerical differences between the iterations are moderate, they are achieved after only a small number of real-vehicle evaluations, despite the controller being treated as a noisy black-box system. This underscores the efficiency of the proposed BO framework: it is able to extract useful structural information from sparse and noisy measurements, guide exploration toward promising regions of the gain space, and progressively refine the controller performance without requiring any analytical model.

In summary, these experiment results demonstrate that BO can handle strongly coupled parameters and noisy experimental data while still converging within a limited evaluation budget. Therefore, the improvements observed in Iteration 31 are the clear evidence that data-efficient BO is well suited for tuning real-world path-following controllers under real-world conditions.

## V. CONCLUSION

This paper presented a BO based framework for automatic tuning of a Lyapunov-based kinematic path-following controller on Honda's AI-Formula three-wheeled robot. The controller contains four strongly coupled gains, making manual tuning unreliable under the limited experimental budget and substantial measurement noise inherent to real-vehicle testing. To address this challenge, the proposed framework employs Bayesian optimization with a GP surrogate and acquisition-driven exploration, enabling systematic gain adaptation from noisy, expensive, and purely black-box closed-loop evaluations.

Real-world experiments on the AI-Formula track demonstrate the effectiveness and efficiency of the proposed approach. Using a total of 32 closed-loop evaluations, including 15 warm-start initial trials, the BO process achieved a clear improvement in the performance index. Starting from the manually tuned baseline ( $\hat{J}_{BO} = 2076.35$ ), the optimization reached its best value ( $\hat{J}_{BO} = 1887.65$ ) at Iteration 31. Path comparisons show reduced tracking deviations in curved sections of the course, while Table II indicates that the maximum lateral error is reduced by approximately 18–20% relative to Iterations 1 and 9. These results confirm that BO can efficiently explore a noisy, high-dimensional gain space and identify well-performing configurations with far fewer trials than manual tuning would typically allow. In summary, this study demonstrates that BO provides a practical and data-efficient tool for tuning nonlinear controllers on real robotic platforms, especially when accurate modelling is difficult and cost of each experiment is expensive. As future work, we plan to extend the framework to safety-aware Bayesian optimization, where a conservative safety region is maintained and gradually expanded during exploration.

## REFERENCES

- [1] N. A. I. Ruslan, N. H. Amer, K. Hudha, Z. Abdul Kadir, S. A. F. Mohamed Ishak, and S. M. F. Syed Dardin. "Modelling and control strategies in path tracking control for autonomous tracked vehicles: A review of state of the art and challenges," *Journal of Terramechanics*, vol. 105, pp. 67–79, 2023.
- [2] M. Samuel, M. Hussein, and M. B. Mohamad. "A review of some pure-pursuit based path tracking techniques for control of autonomous vehicle,"
- [3] R. P. Borase, D. K. Maghade, S. Y. Sondkar, et al. "A review of PID control, tuning methods and applications," *International Journal of Dynamics and Control*, vol. 9, no. 2, pp. 818–827, 2021.
- [4] Z. Song and Y. Huang. "Review of intelligent motor controller parameter self-tuning technology," *Electronics*, vol. 14, no. 11, p. 2229, 2025.
- [5] M. Rokonuzzaman, N. Mohajer, S. Nahavandi, et al. "Review and performance evaluation of path tracking controllers of autonomous vehicles," *IET Intelligent Transport Systems*, vol. 15, no. 5, pp. 646–670, 2021.
- [6] H. Lee and H. J. Kim. "Trajectory tracking control of multirotors from modelling to experiments: A survey," *International Journal of Control, Automation and Systems*, vol. 15, no. 1, pp. 281–292, 2017.
- [7] I. A. Abbas and M. K. Mustafa. "A review of adaptive tuning of PID-controller: Optimization techniques and applications," *International Journal of Nonlinear Analysis and Applications*, vol. 15, no. 2, pp. 29–37, 2024.
- [8] A. D. Sabiha, M. A. Kamel, E. Said, and W. M. Hussein. "ROS-based trajectory tracking control for autonomous tracked vehicle using optimized backstepping and sliding mode control," *Robotics and Autonomous Systems*, vol. 152, p. 104058, 2022.
- [9] F. M. Kasim and V. R. Jisha. "Lyapunov-based approach for target tracking control of a mobile robot," in *2015 IEEE International Conference on Electrical, Computer and Communication Technologies (ICECCT)*, Coimbatore, India, pp. 1–6, 2015.
- [10] H. Peng, W. Wang, Q. An, C. Xiang, and L. Li. "Path tracking and direct yaw moment coordinated control based on robust MPC with the finite time horizon for autonomous independent-drive vehicles," *IEEE Transactions on Vehicular Technology*, vol. 69, no. 6, pp. 6053–6066, 2020.
- [11] Y. Zhao, Y. Ma, and S. Hu. "USV formation and path-following control via deep reinforcement learning with random braking," *IEEE Transactions on Neural Networks and Learning Systems*, vol. 32, no. 12, pp. 5468–5478, 2021.
- [12] N. H. Amer, H. Zamzuri, K. Hudha, et al. "Modelling and Control Strategies in Path Tracking Control for Autonomous Ground Vehicles: A Review of State of the Art and Challenges," *J Intell Robot Syst*, vol. 86, pp. 225–254, 2017.
- [13] H. Hjalmarsson. "Iterative feedback tuning—an overview," *International Journal of Adaptive Control and Signal Processing*, vol. 16, no. 5, pp. 373–395, 2002.
- [14] S. You, Y. S. Son, Y. Gui, and W. Kim. "Gradient-descent-based learning gain for backstepping controller and disturbance observer of nonlinear systems," *IEEE Access*, vol. 11, pp. 2743–2753, 2023.
- [15] A. R. Kumar and P. J. Ramadge. "DiffLoop: Tuning PID controllers by differentiating through the feedback loop," in *2021 55th Annual Conference on Information Sciences and Systems (CISS)*, Baltimore, MD, USA, pp. 1–6, 2021.
- [16] P. J. Fleming and R. C. Purshouse. "Evolutionary algorithms in control systems engineering: a survey," *Control Engineering Practice*, vol. 10, no. 11, pp. 1223–1241, 2002.
- [17] H. V. H. Ayala and L. dos Santos Coelho. "Tuning of PID controller based on a multiobjective genetic algorithm applied to a robotic manipulator," *Expert Systems with Applications*, vol. 39, no. 10, pp. 8968–8974, 2012.
- [18] D. Maiti, A. Acharya, M. Chakraborty, A. Konar, and R. Janarthanan. "Tuning PID and  $PI^{\lambda}D^{\delta}$  controllers using the integral time absolute error criterion," in *International Conference on Information and Automation*, pp. 457–462, 2008.
- [19] M. Neumann-Brosig, A. Marco, D. Schwarzmann, et al. "Data-efficient autotuning with Bayesian optimization: An industrial control study," *IEEE Transactions on Control Systems Technology*, vol. 28, no. 3, pp. 730–740, 2019.
- [20] J. P. L. Coutinho, L. O. Santos, and M. S. Reis. "Bayesian Optimization for automatic tuning of digital multi-loop PID controllers," *Computers & Chemical Engineering*, vol. 173, p. 108211, 2023.
- [21] B. Shahriari, K. Swersky, Z. Wang, et al. "Taking the human out of the loop: A review of Bayesian optimization," *Proceedings of the IEEE*, vol. 104, no. 1, pp. 148–175, 2015.

- [22] S. Greenhill, S. Rana, S. Gupta, et al. ‘Bayesian optimization for adaptive experimental design: A review,’ *IEEE Access*, vol. 8, pp. 13937–13948, 2020.
- [23] M. Tesch, J. Schneider, and H. Choset. ‘Using response surfaces and expected improvement to optimize snake robot gait parameters,’ in *Proceedings of the 2011 IEEE/RSJ International Conference on Intelligent Robots and Systems (IROS)*, IEEE, pp. 1069–1074, 2011.
- [24] R. Calandra, N. Gopalan, A. Seyfarth, et al. ‘Bayesian gait optimization for bipedal locomotion,’ in *Proceedings of the International Conference on Learning and Intelligent Optimization*, Cham: Springer International Publishing, pp. 274–290, 2014.
- [25] M. Schillinger, B. Hartmann, P. Skalecki, et al. ‘Safe active learning and safe Bayesian optimization for tuning a PI-controller,’ *IFAC-PapersOnLine*, vol. 50, no. 1, pp. 5967–5972, 2017.
- [26] A. Gharib, D. Stenger, R. Ritschel, et al. ‘Multi-objective optimization of a path-following MPC for vehicle guidance: A Bayesian optimization approach,’ in *Proceedings of the 2021 European Control Conference (ECC)*, IEEE, pp. 2197–2204, 2021.
- [27] W. Strózecki, N. Ait Oufroukh, Y. Kebbati, et al. ‘Automatic tuning of MPC for autonomous vehicle using Bayesian optimization,’ in *Proceedings of the 2021 IEEE International Conference on Networking, Sensing and Control (ICNSC)*, IEEE, vol. 1, pp. 1–6, 2021.
- [28] L. P. Fröhlich, C. Küttel, E. Arcari, et al. ‘Contextual tuning of model predictive control for autonomous racing,’ in *Proceedings of the 2022 IEEE/RSJ International Conference on Intelligent Robots and Systems (IROS)*, IEEE, pp. 10555–10562, 2022.
- [29] J. Menn, P. Pelizzari, M. Fleps-Dezasse, et al. ‘Lipschitz safe Bayesian optimization for automotive control,’ in *Proceedings of the 2024 IEEE 63rd Conference on Decision and Control (CDC)*, IEEE, pp. 3782–3788, 2024.
- [30] M. Okada, Y. Akimoto, A. Kato, and Y. Yasui. ‘AI Formula,’ in *Proceedings of the 2024 Spring Conference of the Society of Automotive Engineers of Japan (JSAE) – Academic Lectures*, no. 20245167, 2024.
- [31] M. Veronesi and A. Visioli. ‘Performance assessment and retuning of PID controllers for integral processes,’ *Journal of Process Control*, vol. 20, no. 3, pp. 261–269, 2010.
- [32] M. Chen. ‘Integrated YOLOP perception and Lyapunov-based control for autonomous mobile robot navigation on track,’ *arXiv:2512.01608*, 2025.
- [33] L. Bliek, A. Guijt, R. Karlsson, et al. ‘Benchmarking surrogate-based optimisation algorithms on expensive black-box functions,’ *Applied Soft Computing*, vol. 147, p. 110744, 2023.
- [34] A. Marrel and B. Iooss. ‘Probabilistic surrogate modeling by Gaussian process: A review on recent insights in estimation and validation,’ *Reliability Engineering & System Safety*, vol. 247, p. 110094, 2024.
- [35] J. Snoek, H. Larochelle, and R. P. Adams. ‘Practical Bayesian optimization of machine learning algorithms,’ *Advances in Neural Information Processing Systems*, vol. 25, 2012.
- [36] C. E. Rasmussen. ‘Gaussian processes in machine learning,’ in *Summer School on Machine Learning*, Berlin, Heidelberg: Springer Berlin Heidelberg, pp. 63–71, 2003.



**Zhewen Zheng** Zhewen Zheng received the B.Eng. degree in mechanical design, manufacture, and automation from the University of Shanghai for Science and Technology, Shanghai, China, in 2022, and the M.Eng. degree in the Green Science and Engineering Division from Sophia University, Tokyo, Japan, in 2024. He is currently working toward the Ph.D. degree in the same division at Sophia University and is expected to complete his doctoral program in the fall of 2027. His research interests include path following control of the automobile, automobile powertrain dynamics, optimization theory and its application.



**Wenjing Cao** Wenjing Cao received her Ph.D. degree in engineering from the Graduate School of Integrated Frontier Science, Kyushu University, Japan, in 2014. Subsequently, she joined Nissan Motor Co., Ltd. and worked on the powertrain control of CAVs for four years. She is currently a faculty member in the Department of Engineering and Applied Sciences at Sophia University, Japan. Her current research focuses on control theory and its application to the motion control of automobiles, robots, and the control of automobile powertrains. She is a member of SICE, JSAE, IEEJ, and IEEE.



**Hongkang Yu** Hongkang Yu received the B.Eng. degree and the M.Eng. degree in the Green Science and Engineering Division from Sophia University, Tokyo, Japan. He is currently working toward his Ph.D. degree in the same division at Sophia University and is expected to complete his doctoral program in the fall of 2028. His research interests include control engineering, automated driving, obstacle avoidance, and path planning.



**Takashi Suzuki** Takashi Suzuki is a Professor in the Department of Engineering and Applied Sciences at Sophia University, Tokyo, Japan. He received his Ph.D. degree in 1999 from Sophia University. He has been teaching at Sophia University since 1988. His research contributions include the improvement of thermal efficiency in SI engines, combustion analysis of alternative automotive fuels, and the investigation of boiling flows.